

AltTS: A Dual-Path Framework with Alternating Optimization for Multivariate Time Series Forecasting

Zhihang Yuan ^{*1} Zhiyuan Liu ^{*2} Mahesh K. Marina ¹

Abstract

Multivariate time series forecasting involves two qualitatively distinct factors: (i) stable within-series autoregressive (AR) dynamics, and (ii) intermittent cross-dimension interactions that can become spurious over long horizons. We argue that fitting a single model to capture both effects creates an optimization conflict: the high-variance updates needed for cross-dimension modeling can corrupt the gradients that support autoregression, resulting in brittle training and degraded long-horizon accuracy. To address this, we propose AltTS, a dual-path framework that explicitly decouples autoregression and cross-relation (CR) modeling. In AltTS, the AR path is instantiated with a linear predictor, while the CR path uses a Transformer equipped with Cross-Relation Self-Attention (CRSA); the two branches are coordinated via alternating optimization to isolate gradient noise and reduce cross-block interference. Extensive experiments on multiple benchmarks show that AltTS consistently outperforms prior methods, with the most pronounced improvements on long-horizon forecasting. Overall, our results suggest that carefully designed optimization strategies, rather than ever more complex architectures, can be a key driver of progress in multivariate time series forecasting. The code will be open-sourced upon publication.

1. Introduction

Time series forecasting aims to estimate future outcomes from past observations. Classical multivariate time series analysis rests on structural and probabilistic assumptions that enable tractable inference. Vector autoregression (VAR) offers a concise baseline for joint stationary dynamics (Sims, 1980), while cointegration theory captures co-movements

^{*}Equal contribution ¹School of Informatics, University of Edinburgh, UK ²University of Chicago, USA. Correspondence to: Mahesh K. Marina <mahesh@ed.ac.uk>.

Preprint. February 13, 2026.

among non-stationary series (Engle & Granger, 1987). Modern methodologies further provide systematic approaches for long-horizon, high-dimensional time series with diverse cross-time, cross-variable interactions (Newey & West, 1987; Bai & Ng, 2002; Basu & Michailidis, 2015). In those statistical methods, modeling cross-variable dependencies is fundamental to understanding the multivariate system.

Building on these foundations, recent deep learning methods extend time series modeling and have demonstrated significant scalability and strong inference ability for long-term time series forecasting (LTSF). Representative lines include CNN- and RNN-based (Lai et al., 2017; Li et al., 2018; LIU et al., 2022), graph-based (Yu et al., 2018; Shang et al., 2021), and Transformer-based (Zhou et al., 2021; 2022) models. These models tailor the network structure to the characteristics of time series data, among which techniques such as patching (Nie et al., 2023), sparse modeling (Lin et al., 2024) and dependency modeling (Zhang & Yan, 2023; Hu et al., 2025) have delivered notable gains across various real-world settings. At the same time, the recent success of MLP-based and linear models (Oreshkin et al., 2020; Zeng et al., 2023; Das et al., 2023; Huang et al., 2025) call into question whether increasingly complex architectures are necessary for LTSF, and motivate re-examining how to represent the core properties of multivariate time series for effective forecasting.

From an optimization perspective, training of modern neural networks operates in a non-convex and often non-smooth regime. Foundational analyses establish the convergence of stochastic first-order methods, while adaptive approaches such as Adam (Kingma & Ba, 2015) have inspired refinements and provably convergent variants like AMSGrad (Reddi et al., 2018). For structured objectives, proximal alternating methods (Bolte et al., 2014) and block-coordinate descent (BCD) guarantee monotone descent and convergence, which are attracting growing interest within the deep learning community (Du et al., 2019; Zeng et al., 2019). More broadly, the integration of optimization principles with network design, exemplified by embedding differentiable optimization layers in networks (Amos & Kolter, 2017) and unfolding iterative algorithms for model alignment (Luo et al., 2020), has emerged as a powerful paradigm for taming

ill-conditioned learning dynamics. In the context of LTSF, unstable learning dynamics can originate from heterogeneous dependency structures. Figure 1 reports the variance of gradient for autoregression (AR) and cross-relation (CR) parameters under the joint and the alternating training schedules. Since AR and CR patterns differ in learning difficulty, the two components often require different step sizes to converge. With a shared optimizer in the joint training, the CR block exhibits exploding variance in five of seven datasets, whereas the variance with the AR block remains comparatively low and decays over epochs. The high variance of the CR parameter updates injects non-negligible noise into the entire model. The alternating method mitigates this instability by using separate optimizers for AR and CR, yielding more stable convergence for both paths.

Based on the above observations, we propose AltTS, a dual-path framework that decouples dependency modeling and trains the two paths via alternating optimization. In AltTS, AR and CR are separately forecasted by two modules. Subsequently, alternating optimization is applied to alleviate the entanglement of seemingly homogeneous AR and CR through cyclic block-wise updates. Experimentally, AltTS achieves state-of-the-art performance in a wide range of time series forecasting tasks with minimal architectural sophistication. Our contributions are as follows:

1. We present AltTS, the first deep learning framework that explicitly *decouples* autoregression and cross-variable dependency and coordinates them via *alternating optimization*. Our analysis further reveals the risk of gradient entanglement when these patterns are learned jointly, especially when the true longitudinal structure is unobservable.
2. We evaluate AltTS on seven widely used multivariate time series benchmarks against strong linear, Transformer-based, and hybrid baselines. AltTS consistently achieves competitive or superior performance across datasets and horizons while relying only on canonical architectures, underscoring the effectiveness of optimization-driven design.
3. Beyond empirical results, AltTS highlights that *training schedules can be treated as a design variable*, pointing to new opportunities for integrating optimization principles into the structural design of neural networks.

2. Related Work

Long-Term Time Series Forecasting Transformer-based models have been a dominant thread in long-term time series forecasting (LTSF). Many advancements involve adapting the Transformer (Vaswani et al., 2017) for LTSF. These

models utilize various properties of long-term time series through seasonal-trend decomposition (Wu et al., 2021; Wang et al., 2024), frequency analysis (Zhou et al., 2022; Chen et al., 2024), and sparse modeling (Zhou et al., 2021; Luo & Wang, 2024). Further investigations into the characteristics of time-series data show that simple models, such as linear layers (Zeng et al., 2023; Li et al., 2023), can achieve comparable or superior performance to Transformers. More recently, OLinear (Yue et al., 2025) further demonstrates that linear forecasters can be highly competitive by operating in an orthogonally transformed domain to alleviate entangled temporal dependencies. In parallel, there is a growing interest in dependency modeling. The Channel Independent (CI) methods rely solely on the historical information of each series, individually or through a pooled Channel Mix (CM) modeling, thus concentrating on autoregressive patterns. PatchTST (Nie et al., 2023) proposes a CI/CM patching, showing consistent gains on long horizons. Following this path, pure autoregressive models including TimesNet (Wu et al., 2023), SparseTSF (Lin et al., 2024), and TimeBase (Huang et al., 2025) achieve impressive performance, demonstrating the effectiveness of CI modeling. However, the CI/CM modeling overlooks cross-variable dependency, leading to a fundamental deviation of the learned model from the actual data-generating processes. In contrast, the Channel Dependent (CD) methods explicitly target cross-dimension structures. Crossformer (Zhang & Yan, 2023) designs a two-stage attention to capture cross-time and cross-dimension dependencies. iTransformer (Liu et al., 2023) tokenizes variables and applies attention to their time embeddings, where attention scores implicitly represent multivariate correlations. To resolve the high variable dimensionality in large datasets, Channel Clustering (CC) is proposed, analogous to patching in time domain modeling. In CC methods, such as DUET (Qiu et al., 2025) and Time-Filter (Hu et al., 2025), heterogeneous variables are grouped together to preserve instantaneous correlations. The two-stage temporal-spatial paradigm is widely adopted in most CD methods. While recent studies also experiment on structures compatible with both CI and CD settings (Lin et al., 2025), further research on the integration of autoregressive and cross-dimension modeling is still needed.

Alternating Optimization Alternating optimization methods attract increasing interest in deep learning, such as Block-Coordinate Descent (BCD) and Alternating Direction Method of Multipliers (ADMM) by Boyd et al. (2010). Algorithms that allow general non-smooth and non-convex problems provide theoretical foundations for the application in deep learning scenarios (Razaviyayn et al., 2013; Bolte et al., 2014; Razaviyayn et al., 2014). Meanwhile, the alternating optimization algorithms are employed heuristically in adversarial learning (Goodfellow et al., 2014) and Computer Vision (Luo et al., 2020; Akbari et al., 2023), where

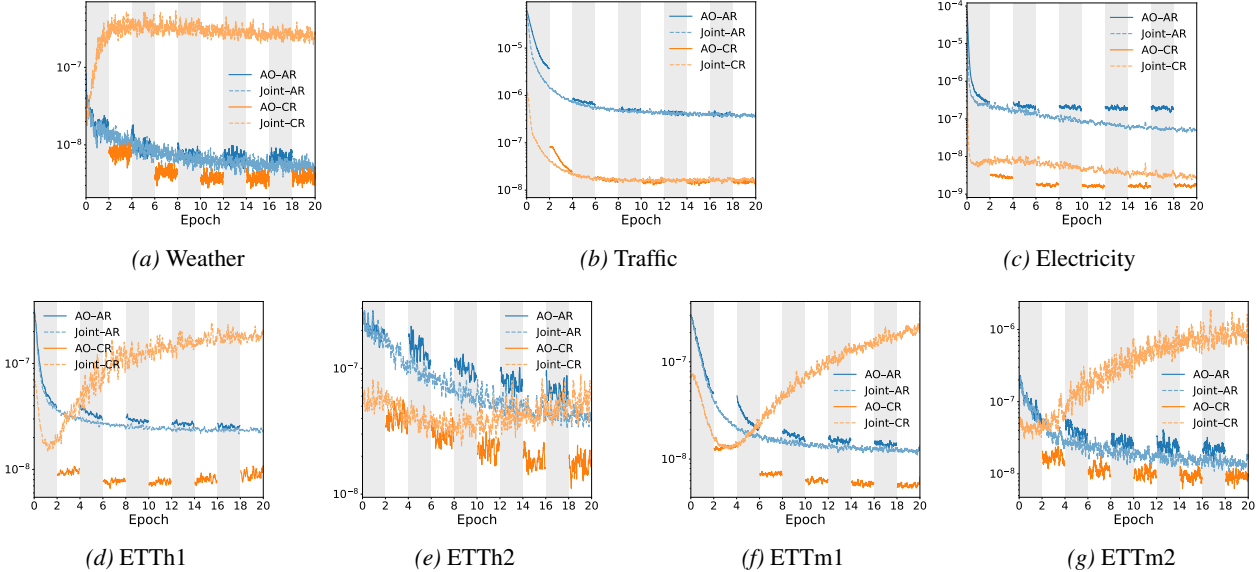


Figure 1. Variance of AR/CR gradients under *alternating* vs. *joint* training on seven datasets (prediction length = 96). The y-axis is the natural log of the gradient variance statistic. We compute the rolling sample variance of gradients for each parameter over the last K updates; within each branch, we take the parameter-wise sum to yield a scalar for AR and CR in the rolling window, respectively. Extended plots for horizons 192/336/720 are in Appendix B.

two or more neural networks and objectives are alternately optimized for better alignment. In this paper, we explore the alternating optimization of dependency modeling schemes for LTSF to coordinate autoregressive and cross-dimension patterns while preserving temporal causality.

3. Methodology

3.1. General Structure

In the multivariate time series forecasting task, let $\mathbf{X}_t = [\mathbf{x}_t^{(1)}, \dots, \mathbf{x}_t^{(D)}] \in \mathbb{R}^{D \times L}$ be the lookback window at step t , where each $\mathbf{x}_t^{(i)} = [x_{t-L+1}^{(i)}, \dots, x_t^{(i)}]$ represents a historical input sequence of length L . D denotes the number of dimensions. The target sequence is $\mathbf{Y}_{t+1} = [\mathbf{y}_{t+1}^{(1)}, \dots, \mathbf{y}_{t+1}^{(D)}] \in \mathbb{R}^{D \times H}$, where $\mathbf{y}_{t+1}^{(i)} = [x_{t+1}^{(i)}, \dots, x_{t+H}^{(i)}]$ is the realization of the i -th sequence from step $t+1$ to $t+H$. For the individual sequences, we omit the subscript t and use $\mathbf{x}_i := \mathbf{x}_t^{(i)}$, $\mathbf{y}_i := \mathbf{y}_{t+1}^{(i)}$ for short in the following analysis.

In general, to generate the predicted series $\hat{\mathbf{Y}}_{t+1}$, a transition matrix is used. Let $\mathbf{F} = (f_{ij})_{D \times D}$ be a matrix of projections. Each projection $f_{ij} : \mathbb{R}^L \mapsto \mathbb{R}^H$ measures the contribution of \mathbf{x}_j to \mathbf{y}_i . \mathbf{F} , f_{ij} can be approximated by a neural network or part of a neural network, denoted by $\hat{\mathbf{F}}$ and \hat{f}_{ij} respectively. For convenience, we define an

“apply-then-sum” operator $*$ as

$$\mathbf{F} * \mathbf{X}_t := \left(\sum_{j=1}^D f_{1j}(\mathbf{x}_j), \dots, \sum_{j=1}^D f_{Dj}(\mathbf{x}_j) \right) \in \mathbb{R}^{D \times H}. \quad (1)$$

Note that the $*$ operation is linear with respect to the first argument. The transition equation is therefore

$$\mathbf{F} * \mathbf{X}_t + \mathbf{V}_{t+1} = \mathbf{Y}_{t+1}, \quad (2)$$

where \mathbf{V}_{t+1} represents the unpredictable innovations of the time series at step $t+1$ given \mathbf{X}_t . This general form summarizes CI, CM, and CD methods. Setting all off-diagonal projections to zero, $f_{ij} \equiv 0$, $i \neq j$ yields the CI methods, where D independent neural networks are used to model the autoregression per series. Further imposing $f_{11} = \dots = f_{DD}$ gives the CM setting, where a single shared neural network generalizes the autoregressive patterns from all series. Allowing non-trivial off-diagonal entries, i.e., at least one f_{ij} , $i \neq j$ depends on the input, leads to the CD methods with explicit cross-dimension effects.

However, the fully dense specification is computationally inefficient and susceptible to overfitting, especially when each f_{ij} is independently parameterized. To better utilize the cross-variable structure, recent work adopts Channel Clustering (CC), which is equivalent to a block-diagonal constraint to \mathbf{F} . Essentially, the $D \times D$ entries of \mathbf{F} are estimated by a significantly smaller number of modules, reflecting the low intrinsic dimensionality of many long-horizon high-dimensional time series. Through different grouping

and coupling schemes for $\{f_{ij}\}$, one can instantiate different structural assumptions on inter-series dependence.

3.2. AR-CR Structural Decoupling

Modeling cross-dimension dependencies is challenging in multivariate forecasting. Autoregression (AR) is typically stable and persistent, whereas cross-relations (CR) are often regime-dependent and instantaneous. However, most dependency modeling methods either discard CR completely or homogeneously model the two. Empirically (Fig. 1), joint optimization yields persistently higher gradient variance for CR, while AR gradients are smaller and mostly monotonically decaying. The high-variance CR updates inject non-negligible noise into the whole model, indicating different step-size/curvature needs; a shared optimizer entangles updates and lets CR noise bleed into AR, hindering convergence. These observations motivate a decoupled parameterization and training schedule.

We therefore propose a dual-path design that explicitly separates AR and CR modeling, as illustrated in Figure 2. Rather than estimating the full operator at once, we break down \mathbf{F} into diagonal and off-diagonal components, $\mathbf{F} = \mathbf{F}_{\text{AR}} + \mathbf{F}_{\text{CR}}$, due to their distinct properties. $\mathbf{F}_{\text{AR}} = \text{diag}(f_{11}, \dots, f_{DD})$ captures per-series AR patterns, and $\mathbf{F}_{\text{CR}} = \mathbf{F} - \mathbf{F}_{\text{AR}}$ encodes all cross-dimension dependencies.

Auto-Regression Path. For each variable i , we first apply Reversible Instance Normalization, RevIN (Kim et al., 2021), and fit a linear predictor \hat{f}_{ii}

$$\hat{y}_i^{\text{AR}} = \hat{f}_{ii}(\mathbf{x}_i) \quad (3)$$

Parameters are not shared across i , enforcing channel independence. The AR path coincides with the RLinear model (Li et al., 2023). This simple model provides a clean separation of autoregression from cross-dimension effects. The AR path is trained with L1 regularization to prevent overfitting in long-horizon modeling.

Cross-Relation Path. We apply an inverted Transformer encoder that attends across variables. To prevent leakage of AR information into the CR module, we mask intra-series links in the attention matrix. Each individually normalized time series is compressed into a L_0 -dimensional token via a linear projection,

$$\mathbf{Z}_0 = \text{Embedding}(\mathbf{X}_t) \quad (4)$$

where $\mathbf{Z}_0 \in \mathbb{R}^{D \times L_0}$ denotes the temporal embeddings of variables. \mathbf{Z}_0 is passed into the Multi-Head Self-Attention (MHSA) layer (Vaswani et al., 2017). For each head, the Cross-Relation Self-Attention (CRSA) is calculated as

$$\text{CRSA}(\mathbf{Z}_0) = \text{softmax}\left(\frac{\mathbf{Q}\mathbf{K}^\top}{\sqrt{d_h}} + \mathbf{M}\right)\mathbf{V} \quad (5)$$

where $\mathbf{Q}, \mathbf{K}, \mathbf{V} \in \mathbb{R}^{D \times d_h}$ denote queries, keys, and values, respectively. The attention learns *cross-variable* rather than cross-time dependencies. As such, the attention matrix $\mathbf{A} = (\mathbf{Q}\mathbf{K}^\top/\sqrt{d_h})$ represents the multivariate correlations, same as iTransformer (Liu et al., 2023). The additional mask $\mathbf{M} = \text{diag}(-\infty, \dots, -\infty)$ zeros out diagonal attention weights in CRSA. This prevents the CR module from duplicating the AR function, thus enforcing a CR-only modeling. The remainder of the encoder follows the standard Transformer block Vaswani et al. (2017)

$$\begin{aligned} \mathbf{Z}_1 &= \text{LayerNorm}(\mathbf{Z}_0 + \text{MHSA}(\mathbf{Z}_0)) \\ \mathbf{Z}_2 &= \text{LayerNorm}(\mathbf{Z}_1 + \text{MLP}(\mathbf{Z}_1)) \end{aligned} \quad (6)$$

where MLP denotes a two-layer feedforward network. A channel-independent linear head maps the encoder output to the CR components \hat{y}_i^{CR} in the target sequence.

The final output is the denormalized sum of the AR and CR outputs. Our implementation uses a parameter-free RevIN layer, so the two paths share no trainable parameters.

3.3. Block Alternating Optimization

Gradient Entanglement of Joint AR-CR Training. For simplicity, the following discussion considers the MSE loss function under minibatch optimization, so gradients are stochastic. With perfect knowledge of cross-variable contributions $f_{ij}, j = 1, \dots, D$ for each variable i , the gradient for \hat{f}_{ij} can be estimated as

$$\nabla_{\theta_{ij}} \mathcal{L}^* = -J_{ij}^\top \mathbf{r}_{ij}, \quad (7)$$

where $\mathcal{L}^* := \frac{1}{2} \sum_{i,j=1}^D \|\mathbf{r}_{ij}\|_2^2$. θ_{ij} is the set of parameters for \hat{f}_{ij} , J_{ij} is the Jacobian, and $\mathbf{r}_{ij} := f_{ij}(\mathbf{x}_j) - \hat{f}_{ij}(\mathbf{x}_j)$ is the residual of the fitted projection \hat{f}_{ij} . Because (7) is additively separable across i, j , the update is unaffected by other projections. The learned \hat{f}_{ij} is therefore consistent with the true projection f_{ij} .

However, in real-world time series forecasting, such decomposition of residuals is infeasible. Without access to the true transition matrix \mathbf{F} , we only observe the aggregate residuals $\mathbf{r}_i := \mathbf{y}_i - \hat{\mathbf{y}}_i = \sum_{j=1}^D \mathbf{r}_{ij}, i = 1, \dots, D$. The estimated gradient mixes estimation errors from multiple projections,

$$\nabla_{\theta_{ij}} \mathcal{L} = -J_{ij}^\top \mathbf{r}_i, \quad (8)$$

where $\mathcal{L} := \frac{1}{2} \sum_{i=1}^D \|\mathbf{r}_i\|_2^2$. Minimizing the sum of $\|\mathbf{r}_i\|_2^2$ does not guarantee the consistency between each individual \hat{f}_{ij} and f_{ij} , but only the combined mapping over j . Equation 8 induces gradient entanglement between parameter blocks θ_{ii} and θ_{ij} through the shared residual \mathbf{r}_i throughout training. When series are relatively homogeneous and exhibit spurious correlations, joint training can couple the AR and CR updates, blurring the intended separation between

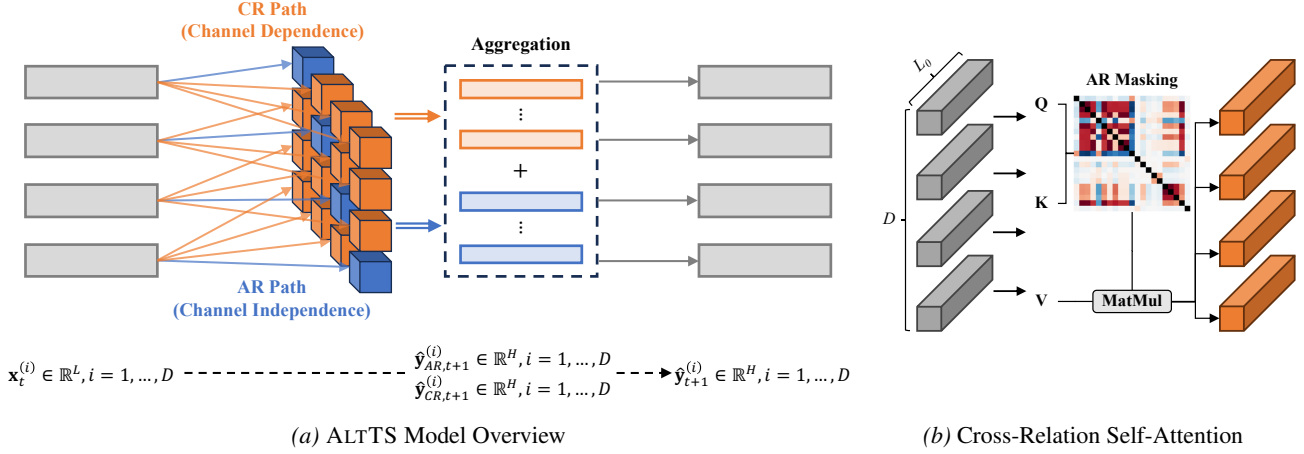


Figure 2. Architecture of ALTTS. (a) Multivariate time series is passed into two parallel paths, the channel-independent AR path and the channel-dependent CR path. Outputs are summed to obtain the final prediction. (b) The cross-relation self-attention forms queries/keys/values from per-variable embeddings and an AR mask is applied to the attention matrix to suppress intra-series links.

temporal autoregression and cross-variable modeling (as shown in Figure 1 and Appendix B), and often biasing optimization toward cross-variable signals when correlations are strong but weakly informative.

Let $\mathbf{r}_{-ii} := \sum_{j \neq i}^D \mathbf{r}_{ij}$ be the sum of CR residuals for variable i . For each AR projection \hat{f}_{ii} , the unbiasedness of (8) requires the conditional expectation of the bias term to be zero.

$$\mathbb{E}(-J_{ii}^\top \mathbf{r}_{-ii} \mid \mathbf{x}_i) = -J_{ii}^\top \mathbb{E}(\mathbf{r}_{-ii} \mid \mathbf{x}_i) = 0, \quad (9)$$

which requires $\mathbb{E}(\mathbf{r}_{-ii} \mid \mathbf{x}_i) = 0$. However, due to the existence of cross-variable dependencies and the shared residual \mathbf{r}_i among \hat{f}_{ij} , this requirement fails to hold unless projections $\hat{f}_{ij}, j \neq i$ are constant with respect to \mathbf{x}_i as in the CI setting. In the general CD setting, where $\mathbb{E}(\mathbf{x}_j \mid \mathbf{x}_i) \neq 0$ for some j , $\mathbb{E}(\mathbf{r}_{-ii} \mid \mathbf{x}_i)$ is a non-trivial function of \mathbf{x}_i .

The bias in the mixed gradient may not pose a problem for forecasting since unbiased predictions can still be attainable. Nonetheless, it can degrade training stability. Conditional on \mathbf{x}_i , the covariance of (7) is 0, whereas the covariance of the mixed gradient (8), $\text{Cov}(-J_{ii}^\top \mathbf{r}_i \mid \mathbf{x}_i) = \text{Cov}(-J_{ii}^\top \mathbf{r}_{-ii} \mid \mathbf{x}_i) \succeq 0$, is generally non-trivial. This additional covariance introduced by the CR contamination translates into noisier updates for the AR block. We consider the following assumption to investigate the unconditional covariance.

Assumption 3.1. Let $\Sigma_{ii} := \text{Cov}(-J_{ii}^\top \mathbf{r}_{ii})$, $\Sigma_{-ii} := \text{Cov}(-J_{ii}^\top \mathbf{r}_{-ii})$ be the covariance matrices of the true gradient and the CR contamination respectively. Assume the covariances satisfy

$$\|\Sigma_{-ii}\|_1 > 4\|\Sigma_{ii}\|_1, \quad (10)$$

where $\|\cdot\|_1$ is the trace norm.

The trace norm of gradient covariance serves as a metric for update turbulence, with the same definition as in Johnson & Zhang (2013); Agarwal et al. (2022). Equation 10 suggests a lower bound for $\|\Sigma_{-ii}\|_1$ when the CR gradient variance is sufficiently large to affect the optimization of the AR path under various settings.

When a subset of variables in the input sequence is highly correlated, the indistinguishability arises and can lead to equation 10. For instance, in a bivariate case with an instantaneous relationship $\mathbf{x}_i = \alpha \mathbf{x}_j + \epsilon, \forall t$ for some constant α while cross-dimension contributions are zero (i.e., $f_{ij} = f_{ji} = 0$), $\|\Sigma_{-ii}\|_1$ can be inflated by misspecified \hat{f}_{ij} . Even without extreme dependence, small cross-dimension errors that arise intermittently can accumulate and materially raise gradient variance over training. To assess its impact on the AR gradient stability, consider the conditional covariance matrix of (8)

$$\text{Cov}(J_{ii}^\top \mathbf{r}_i) = \Sigma_{ii} + \Sigma_{-ii} + 2\text{Cov}(J_{ii}^\top \mathbf{r}_{ii}, J_{ii}^\top \mathbf{r}_{-ii}). \quad (11)$$

The trace norm of equation 11 satisfies

$$\begin{aligned} \|\text{Cov}(J_{ii}^\top \mathbf{r}_i)\|_1 &= \|\Sigma_{ii}\|_1 + \|\Sigma_{-ii}\|_1 \\ &\quad + 2\text{Tr}(\text{Cov}(J_{ii}^\top \mathbf{r}_{ii}, J_{ii}^\top \mathbf{r}_{-ii})) \\ &\geq \|\Sigma_{ii}\|_1 + \|\Sigma_{-ii}\|_1 - 2\sqrt{\|\Sigma_{ii}\|_1 \|\Sigma_{-ii}\|_1} \\ &> \|\Sigma_{ii}\|_1. \end{aligned}$$

The first inequality uses the Cauchy-Schwarz inequality for covariance, with equality if and only if the true AR gradient $-J_{ii}^\top \mathbf{r}_{ii}$ and the CR contamination $-J_{ii}^\top \mathbf{r}_{-ii}$ are perfectly negatively correlated. The second inequality directly follows from assumption 3.1. Hence, the mixed AR gradient is strictly less stable than the true AR gradient.

Alternating Training Strategy. To mitigate gradient entanglement, we separately optimize the AR and CR paths. Specifically, we repeat a two-step alternating optimization (AO) cycle until convergence.

- Step 1. $\theta_{\text{AR}}^{(n+1)} \leftarrow \arg \min_{\theta_{\text{AR}}} \|\mathbf{Y}_{t+1} - (\mathbf{F}_{\text{AR}} + \mathbf{F}_{\text{CR}}^{(n)}) * \mathbf{X}_t\|_2^2 + R_{\text{AR}}(\theta_{\text{AR}})$.
- Step 2. $\theta_{\text{CR}}^{(n+1)} \leftarrow \arg \min_{\theta_{\text{CR}}} \|\mathbf{Y}_{t+1} - (\mathbf{F}_{\text{AR}}^{(n+1)} + \mathbf{F}_{\text{CR}}) * \mathbf{X}_t\|_2^2 + R_{\text{CR}}(\theta_{\text{CR}})$.

$R_{\text{AR}}(\cdot)$ and $R_{\text{CR}}(\cdot)$ are regularizers for the AR module and the CR module, respectively. In practice, we initialize two independent AMSGrad optimizers (Reddi et al., 2018). During training, we first activate the AR regularizer and optimize the AR parameters while keeping the CR parameters frozen; we then alternate the regularizer and freeze the AR parameters to optimize the CR parameters. Each subproblem is run for a small but non-trivial number of inner epochs on the entire training set before alternating. We use AMSGrad due to its convergence guarantee, aligning with alternating optimization algorithms that require sufficient descent and convergence of each subproblem (Razaviyayn et al., 2013; Bolte et al., 2014). For the same reason, we always update the AR path prior to the CR path, since the AR path uses a simpler model in our setting.

The proposed alternating training strategy isolates the two parameter blocks. Intuitively, each subproblem is easier to optimize than the original joint problem due to reduced dimensionality. It also enables distinct learning schedules tailored to AR and CR, which may intrinsically require different step sizes and regularization. The following proposition formalizes the stability benefit of alternating updates.

Proposition 3.2. Suppose the loss function $\mathcal{L}(\theta_{\text{AR}}, \theta_{\text{CR}}; B) = \ell(\theta_{\text{AR}}, \theta_{\text{CR}}; B) + R_{\text{AR}}(\theta_{\text{AR}}) + R_{\text{CR}}(\theta_{\text{CR}})$ is the same under alternating and joint training, where B denotes a random minibatch. Let $\text{Cov}_{\text{alt}}(\nabla_{\theta_{ii}} \mathcal{L})$ be the covariance matrix of gradients for θ_{ii} under alternating training. Then $\text{Cov}_{\text{alt}}(\nabla_{\theta_{ii}} \mathcal{L}) \preceq \text{Cov}(\nabla_{\theta_{ii}} \mathcal{L})$, where $\text{Cov}(\nabla_{\theta_{ii}} \mathcal{L})$ is the joint training gradient covariance.

Note that since $\nabla_{\theta_{ii}} R_{\text{CR}}(\theta_{\text{CR}}) = 0$, using \mathcal{L} is equivalent to applying the loss function in Step 1 when updating the AR path, and vice versa. By the law of total covariance, the gradient covariance under the joint training of θ_{ii} is

$$\text{Cov}(\nabla_{\theta_{ii}} \mathcal{L}) = \mathbb{E}_{\theta_{\text{CR}}}(\text{Cov}(\nabla_{\theta_{ii}} \mathcal{L} \mid \theta_{\text{CR}})) + \text{Cov}_{\theta_{\text{CR}}}(\mathbb{E}(\nabla_{\theta_{ii}} \mathcal{L} \mid \theta_{\text{CR}})). \quad (12)$$

In Step 1 of alternating training, θ_{CR} is held fixed, so the gradient covariance for θ_{ii} is $\text{Cov}(\nabla_{\theta_{ii}} \mathcal{L} \mid \theta_{\text{CR}})$. Taking the expectation over the distribution of θ_{CR} yields

$$\text{Cov}_{\text{alt}}(\nabla_{\theta_{ii}} \mathcal{L}) = \mathbb{E}_{\theta_{\text{CR}}}(\text{Cov}(\nabla_{\theta_{ii}} \mathcal{L} \mid \theta_{\text{CR}})), \quad (13)$$

which is precisely the first term in equation 12. The between-path source of gradient variability is removed. This particularly benefits the AR path, as the CR path usually has noticeably more parameters and slower convergence, making the second term in equation 12 non-negligible.

4. Experiments

4.1. Experimental Overview

We conduct experiments on standard long-term time series forecasting benchmarks to evaluate the effectiveness of decoupling autoregressive and cross-variable modeling via alternating optimization. Specifically, we examine whether alternating optimization improves forecasting accuracy over joint training, whether the gains are consistent across datasets and horizons, and how AltTS compares with recent state-of-the-art linear and attention-based baselines. We further analyze optimization behavior using gradient statistics to elucidate the impact of alternating updates.

4.2. Experimental Setup

Datasets. We evaluate on seven standard LTSF benchmarks: **Weather**, **Traffic**, **Electricity**, and the ETT family (**ETTh1**, **ETTh2**, **ETTm1**, **ETTm2**). Each dataset is chronologically split into train/validation/test sets, and we forecast horizons of $\{96, 192, 336, 720\}$ steps. The input length is fixed to 512, following the convention of PatchTST (Nie et al., 2023). This setting provides a sufficiently long receptive field to capture both autoregressive stability and cross-variable interactions. Detailed dataset descriptions and statistics are provided in Appendix A.

Baselines. We benchmark against representative methods spanning different modeling paradigms: **RLinear** (Li et al., 2023) and **DLinear** (Zeng et al., 2023) (channel-independent/pooled linear models), **PatchTST** (Nie et al., 2023) (patch-based CI/CM Transformer), **iTransformer** (Liu et al., 2023) (variable-token attention for cross-variable modeling), **Informer** (Zhou et al., 2021) (sparse attention), **Time-Base** (Huang et al., 2025) (autoregression-centric backbone), and **OLinear** (Yue et al., 2025), a recent SOTA linear forecaster operating in an orthogonally transformed domain. These baselines cover both autoregressive and cross-variable approaches, providing a comprehensive set of alternative state-of-the-art approaches to evaluate our framework.

Implementation Details. In our dual-path framework, we instantiate the **AR path with RLinear** (Li et al., 2023) and the **CR path with iTransformer** (Liu et al., 2023), aiming to highlight the effect of *alternating optimization* rather than architectural refinements. This instantiation is chosen for clarity rather than necessity: RLinear and iTransformer form a clean decomposition between autoregressive and cross-

Table 1. Full Results. Comparison across seven datasets (Weather, Traffic, Electricity, ETTh1, ETTh2, ETTm1, ETTm2) and four prediction horizons (96/192/336/720). Columns are ordered as *Ours*, OLinear, TimeBase, iTransformer, RLinear, PatchTST, DLinear, and Informer. Metrics are MSE and MAE (lower is better). **Bold** numbers denote the best (lowest) performance in each row, while underlined numbers denote the second best.

Model		Ours		OLinear		TimeBase		iTransformer		RLinear		PatchTST		DLinear		Informer	
Metrics	Model	MSE	MAE	MSE	MAE	MSE	MAE	MSE	MAE	MSE	MAE	MSE	MAE	MSE	MAE	MSE	MAE
Weather	96	0.144	0.195	<u>0.147</u>	0.188	0.151	0.204	0.168	0.218	0.171	0.223	0.150	0.205	0.170	0.229	0.350	0.410
	192	0.192	0.241	<u>0.193</u>	0.244	0.195	0.248	0.210	0.255	0.216	0.260	0.194	<u>0.242</u>	0.215	0.275	0.420	0.430
	336	0.240	0.281	0.247	0.276	0.244	0.282	0.260	0.291	0.261	0.294	<u>0.242</u>	0.283	0.258	0.309	0.580	0.549
	720	0.310	<u>0.329</u>	0.320	0.333	0.317	0.336	0.331	0.341	0.323	0.339	0.314	<u>0.332</u>	0.319	0.359	0.920	0.699
Traffic	96	<u>0.355</u>	0.252	0.341	0.221	0.392	0.259	0.367	0.272	0.395	0.272	0.360	0.253	0.394	0.274	0.739	0.412
	192	<u>0.378</u>	0.265	0.368	0.233	0.413	0.274	0.382	0.269	0.407	0.276	0.379	<u>0.256</u>	0.406	0.279	0.777	0.435
	336	0.395	0.275	0.396	0.242	0.427	0.287	0.395	0.279	0.416	0.282	0.397	<u>0.264</u>	0.415	0.285	0.775	0.450
	720	0.429	0.289	0.491	0.274	0.466	0.301	0.431	0.290	0.454	0.302	0.432	0.292	0.453	0.307	0.820	0.460
Electricity	96	0.131	0.227	0.133	0.220	0.136	0.229	0.132	0.228	0.139	0.244	0.129	<u>0.222</u>	0.135	0.232	0.300	0.399
	192	0.148	<u>0.242</u>	0.154	0.244	0.159	0.255	0.153	0.248	0.150	0.243	0.147	0.240	0.149	0.245	0.327	0.418
	336	0.162	0.258	0.168	0.260	0.172	0.288	0.168	0.265	0.166	0.260	0.163	<u>0.259</u>	0.164	0.265	0.334	0.432
	720	0.204	0.292	0.194	0.283	0.219	0.301	0.195	<u>0.286</u>	0.212	0.300	0.197	0.290	0.198	0.295	0.356	0.429
ETTh1	96	0.360	0.391	0.366	0.400	0.384	<u>0.392</u>	0.399	0.425	0.367	0.394	0.370	0.400	0.378	0.404	0.932	0.766
	192	0.397	0.415	0.407	0.427	0.432	0.462	0.426	0.442	0.402	0.422	0.412	0.428	0.405	<u>0.417</u>	1.001	0.780
	336	0.411	0.429	0.432	0.444	0.445	0.473	0.457	0.464	0.419	0.617	0.421	0.439	0.452	0.457	1.030	0.780
	720	0.435	0.453	0.452	0.470	0.449	0.482	0.630	0.574	0.451	0.463	0.447	0.467	0.502	0.513	1.139	0.852
ETTh2	96	0.273	0.340	0.277	0.337	0.401	0.439	0.297	0.356	<u>0.275</u>	0.341	0.279	0.341	0.282	0.348	1.542	0.957
	192	0.330	0.381	0.351	0.383	0.451	0.467	0.377	0.405	<u>0.336</u>	0.371	0.341	0.383	0.359	0.403	3.791	1.522
	336	0.333	0.392	0.370	0.402	0.458	0.482	0.424	0.440	0.324	<u>0.385</u>	0.328	0.383	0.440	0.454	4.200	1.640
	720	0.375	0.419	0.408	0.437	0.502	0.510	0.438	0.461	0.415	0.445	0.379	<u>0.422</u>	0.608	0.560	3.660	1.620
ETTm1	96	0.290	0.337	0.279	0.338	0.314	0.356	0.311	0.365	0.310	0.351	0.294	0.346	0.304	0.348	0.626	0.549
	192	0.332	0.360	0.334	<u>0.362</u>	0.339	0.370	0.348	0.385	0.338	0.367	0.333	0.370	0.336	0.367	0.725	0.621
	336	0.365	0.380	0.367	0.387	0.374	0.392	0.379	0.405	0.369	<u>0.385</u>	0.370	0.392	0.374	0.395	1.002	0.745
	720	0.423	0.412	0.407	0.417	0.424	0.425	0.443	0.444	0.429	<u>0.415</u>	0.425	0.419	0.427	0.425	1.139	0.841
ETTm2	96	0.160	0.249	0.162	0.250	0.167	0.257	0.178	0.272	0.163	0.251	0.166	0.256	0.165	0.256	0.352	0.467
	192	0.214	0.286	0.219	<u>0.287</u>	0.221	0.293	0.241	0.315	<u>0.217</u>	0.292	0.223	0.296	0.226	0.306	0.599	0.579
	336	0.270	0.324	0.272	0.328	0.273	0.327	0.290	0.344	<u>0.271</u>	0.326	0.273	0.329	0.274	0.335	1.277	0.882
	720	0.357	0.382	0.345	0.372	0.368	0.389	0.376	0.397	0.360	0.387	0.361	0.385	0.380	0.408	2.892	1.219
Count		49		25		1		4		13		19		1		0	

variable modeling, which allows us to isolate the effect of alternating optimization. More generally, our framework is **architecture-agnostic**: both the AR and CR components can be replaced by alternative modules without modifying the optimization procedure. RLinear cleanly models channel-wise autoregression, while iTransformer captures cross-variable dependencies via variable-level self-attention. Both paths use RevIN normalization and are additively combined after denormalization. We adapt Alternating Optimization (AO) in training: AR parameters are updated with CR frozen and vice versa on each mini-batch, each subproblem optimized by AMSGrad with early stopping. We fix the AO schedule to **10 AR updates and 2 CR updates** per mini-batch, reflecting the greater stability of autoregressive dynamics and the higher variance of cross-variable modeling. We scale $R_{\text{AR}}(\cdot)$ and $R_{\text{CR}}(\cdot)$ by prediction length to account for the sensitivity of the ℓ_1 regularizer to parameter count.

Metrics. We report Mean Squared Error (MSE) and Mean Absolute Error (MAE) averaged across all variates, following LTSF conventions. Lower values indicate better predictive performance.

4.3. Main Results

Table 1 summarizes results across all datasets and horizons. **Overall, AltTS attains SOTA or second-best perfor-**

mance on the vast majority of settings. Quantitatively, across all datasets, horizons, and both metrics (56 evaluation slots), AltTS achieves the strongest overall performance with 49 top-two finishes (25 best + 24 second-best), substantially outperforming all baselines. The closest competitor, OLinear, attains 25 top-two results, followed by PatchTST with 19. On the *ETT family*, AltTS is consistently strong—SOTA on ETTh1 (all horizons) and ETTm2 (all horizons), SOTA on ETTh2 at 96/192 and 720 (both metrics), and SOTA/runner-up on ETTm1 (SOTA at 96/192/336; best MAE and second-best MSE at 720). On *Weather*, AltTS is SOTA at 96, 192, and 720 on both metrics (and best MSE at 336). On *Electricity*, it is competitive—SOTA at 336 and second-best at 96/192, while iTransformer leads at 720. On *Traffic*, AltTS leads on MSE at 96 and is generally second-best at 192/336; at 720, iTransformer (MSE) and PatchTST (MAE) edge out AltTS. Taken together, these results show that decoupling AR and CR, paired with alternating optimization, reliably improves stability and accuracy, with the clearest gains on ETT and Weather, especially at longer horizons.

4.4. Ablation Studies

We conduct ablation studies to better understand the contributions of the two key components in our framework: the decoupled AR and CR paths, and the alternating optimization strategy. The first set of experiments disentangle the

Table 2. Ablation study of our framework trained with alternating optimization (w/ AO) and with joint optimization of AR and CR (w/o AO). Each cell shows MSE/MAE; bold indicates the better value per metric.

(a) ETTh1, ETTh2, ETTm1, ETTm2

Horizon (steps)	ETTh1		ETTh2		ETTm1		ETTm2	
	w/ AO	w/o AO						
96	0.360/0.391	0.437/0.453	0.273/0.341	0.321/0.381	0.290/0.338	0.316/0.364	0.160/0.249	0.175/0.263
192	0.397/0.415	0.471/0.473	0.330/0.381	0.371/0.414	0.331/0.360	0.359/0.387	0.214/0.286	0.243/0.313
336	0.411/0.429	0.472/0.479	0.333/0.392	0.374/0.426	0.365/0.380	0.392/0.406	0.270/0.324	0.289/0.341
720	0.435/0.453	0.510/0.506	0.375/0.419	0.440/0.463	0.423/0.412	0.449/0.433	0.357/0.382	0.381/0.401

(b) Electricity, Traffic, Weather

Horizon (steps)	Electricity		Traffic		Weather	
	w/ AO	w/o AO	w/ AO	w/o AO	w/ AO	w/o AO
96	0.131/0.227	0.137/0.233	0.355/0.252	0.364/0.258	0.144/0.195	0.157/0.211
192	0.148/0.242	0.161/0.256	0.380/0.265	0.386/0.269	0.192/0.241	0.203/0.253
336	0.162/0.258	0.179/0.274	0.395/0.275	0.396/0.274	0.240/0.281	0.249/0.288
720	0.204/0.292	0.198/0.291	0.429/0.292	0.481/0.301	0.310/0.329	0.321/0.339

effect of each path by comparing against their standalone counterparts (RLinear and iTransformer), while the second set isolates the role of alternating optimization (AO) by contrasting alternating training with joint optimization. Together, these analyses clarify how architectural decoupling and optimization strategy jointly contribute to the performance of AltTS.

AR vs. CR Path Contributions. To more closely probe the dual-path design, we compare RLinear (AR-only) and iTransformer (CR-only) to AltTS in Table 1. RLinear excels on *Electricity*, where strong periodicity makes per-series autoregression sufficient, but it lags on *Weather* and *Traffic*—datasets where inter-variable structure is essential. Conversely, iTransformer benefits datasets with pronounced cross-variable coupling (e.g., *Weather*, short/mid-horizon *Traffic*) yet underperforms on the *ETT* family, where stable autoregression dominates signal. AltTS reconciles these regimes: the AR path supplies low-variance, persistent dynamics while the CR path selectively captures intermittent cross-relations; alternating optimization coordinates the two so that CR updates do not contaminate AR gradients. Empirically, AltTS achieves best or second-best accuracy in the majority of datasets and horizons, with the largest margins on longer horizons in *ETT* and *Weather*, indicating that AR/CR complementarity—together with alternating updates—yields both greater stability and better forecasting efficacy. These results indicate that alternating optimization is most beneficial when AR and CR signals coexist but compete unevenly, a setting where joint training tends to entangle their gradients and blur their inductive roles.

Effect of Alternating Optimization. Table 2 contrasts alternating optimization (AO) with joint training (single optimizer for AR and CR). Overall, AO lowers both MSE and MAE across datasets and horizons, with the largest gains emerging at long horizons where joint training is most un-

stable (e.g., *ETTh1* at 720: (0.435/0.453) vs. (0.510/0.506)). Improvements are also consistent on *ETTh2*, *ETTm1*, and *ETTm2*, and hold on *Traffic* for short/mid horizons. A few narrow exceptions remain (e.g., *Electricity* at 720 and isolated MAE ties around *Traffic*–336), indicating that while AO is broadly beneficial, extremely CI-friendly regimes can slightly favor joint tuning. These results support our analysis: alternating updates mitigate AR–CR gradient entanglement, yielding more stable optimization and better long-horizon accuracy.

5. Conclusions

In this paper, we have introduced AltTS, a dual-path framework for multivariate time series forecasting that *decouples* autoregression (AR) and cross-relation (CR) modeling and coordinates them via *alternating optimization*. Grounded in an analysis of gradient entanglement under joint AR–CR training, we instantiated the framework with RLinear for AR and modified iTransformer for CR to emphasize optimization over architectural novelty. Across seven multivariate LTSF benchmarks and four horizons, AltTS delivers competitive or superior accuracy, with the largest gains at long horizons where joint training is most unstable. Ablations confirm that AR/CR separation is complementary and that alternating optimization is the key driver of stability and performance. In summary, AltTS is the first deep learning framework to explicitly decouple autoregression and cross-variable dependency via alternating optimization, supported by a theoretical analysis of gradient entanglement. Extensive experiments on seven benchmarks show consistent improvements over strong linear, Transformer-based, and hybrid baselines. Finally, we highlight training schedules as a design variable, suggesting a broader paradigm where optimization principles inform neural network architecture.

References

Agarwal, C., D’souza, D., and Hooker, S. Estimating example difficulty using variance of gradients. In *2022 IEEE/CVF Conference on Computer Vision and Pattern Recognition (CVPR)*, pp. 10358–10368, 2022. doi: 10.1109/CVPR52688.2022.01012.

Akbari, H., Kondratyuk, D., Cui, Y., Hornung, R., Wang, H., and Adam, H. Alternating gradient descent and mixture-of-experts for integrated multimodal perception. In *Thirty-seventh Conference on Neural Information Processing Systems*, 2023.

Amos, B. and Kolter, J. Z. OptNet: Differentiable optimization as a layer in neural networks. In Precup, D. and Teh, Y. W. (eds.), *Proceedings of the 34th International Conference on Machine Learning*, volume 70 of *Proceedings of Machine Learning Research*, pp. 136–145. PMLR, 06–11 Aug 2017.

Bai, J. and Ng, S. Determining the number of factors in approximate factor models. *Econometrica*, 70(1):191–221, 2002. ISSN 00129682, 14680262.

Basu, S. and Michailidis, G. Regularized estimation in sparse high-dimensional time series models. *The Annals of Statistics*, 43(4):1535 – 1567, 2015. doi: 10.1214/15-AOS1315.

Bolte, J., Sabach, S., and Teboulle, M. Proximal alternating linearized minimization for nonconvex and non-smooth problems. *Math. Program.*, 146(1–2):459–494, August 2014. ISSN 0025-5610. doi: 10.1007/s10107-013-0701-9.

Boyd, S., Parikh, N., Chu, E., Peleato, B., and Eckstein, J. Distributed optimization and statistical learning via the alternating direction method of multipliers. *Foundations and Trends in Machine Learning*, 3(1):1–122, 2010. ISSN 1935-8237. doi: 10.1561/2200000016.

Chen, P., Zhang, Y., Cheng, Y., Shu, Y., Wang, Y., Wen, Q., Yang, B., and Guo, C. Pathformer: Multi-scale transformers with adaptive pathways for time series forecasting. In *International Conference on Learning Representations (ICLR)*, 2024.

Das, A., Kong, W., Leach, A., Mathur, S. K., Sen, R., and Yu, R. Long-term forecasting with tiDE: Time-series dense encoder. *Transactions on Machine Learning Research*, 2023. ISSN 2835-8856.

Du, S., Lee, J., Li, H., Wang, L., and Zhai, X. Gradient descent finds global minima of deep neural networks. In Chaudhuri, K. and Salakhutdinov, R. (eds.), *Proceedings of the 36th International Conference on Machine Learning*, volume 97 of *Proceedings of Machine Learning Research*, pp. 1675–1685. PMLR, 09–15 Jun 2019.

Engle, R. F. and Granger, C. W. J. Co-integration and error correction: Representation, estimation, and testing. *Econometrica*, 55(2):251–276, 1987. ISSN 00129682, 14680262.

Goodfellow, I. J., Pouget-Abadie, J., Mirza, M., Xu, B., Warde-Farley, D., Ozair, S., Courville, A., and Bengio, Y. Generative adversarial nets. In Ghahramani, Z., Welling, M., Cortes, C., Lawrence, N., and Weinberger, K. (eds.), *Advances in Neural Information Processing Systems*, volume 27. Curran Associates, Inc., 2014.

Hu, Y., Zhang, G., Liu, P., Lan, D., Li, N., Cheng, D., Dai, T., Xia, S.-T., and Pan, S. Timefilter: Patch-specific spatial-temporal graph filtration for time series forecasting. In *Forty-second International Conference on Machine Learning*, 2025.

Huang, Q., Zhou, Z., Yang, K., Yi, Z., Wang, X., and Wang, Y. Timebase: The power of minimalism in efficient long-term time series forecasting. In *Forty-second International Conference on Machine Learning*, 2025.

Johnson, R. and Zhang, T. Accelerating stochastic gradient descent using predictive variance reduction. In Burges, C., Bottou, L., Welling, M., Ghahramani, Z., and Weinberger, K. (eds.), *Advances in Neural Information Processing Systems*, volume 26. Curran Associates, Inc., 2013.

Kim, T., Kim, J., Tae, Y., Park, C., Choi, J.-H., and Choo, J. Reversible instance normalization for accurate time-series forecasting against distribution shift. In *International Conference on Learning Representations*, 2021.

Kingma, D. P. and Ba, J. Adam: A method for stochastic optimization. In Bengio, Y. and LeCun, Y. (eds.), *ICLR (Poster)*, 2015.

Lai, G., Chang, W.-C., Yang, Y., and Liu, H. Modeling long- and short-term temporal patterns with deep neural networks. *The 41st International ACM SIGIR Conference on Research & Development in Information Retrieval*, 2017.

Li, Y., Yu, R., Shahabi, C., and Liu, Y. Diffusion convolutional recurrent neural network: Data-driven traffic forecasting. In *International Conference on Learning Representations (ICLR ’18)*, 2018.

Li, Z., Qi, S., Li, Y., and Xu, Z. Revisiting long-term time series forecasting: An investigation on linear mapping, 2023.

Lin, S., Lin, W., Wu, W., Chen, H., and Yang, J. Sparseset: Modeling long-term time series forecasting with 1k parameters. *arXiv preprint arXiv:2405.00946*, 2024.

Lin, S., Lin, W., Wu, W., Wang, S., and Wang, Y. Petformer: Long-term time series forecasting via placeholder-enhanced transformer. *IEEE Transactions on Emerging Topics in Computational Intelligence*, 9(2):1189–1201, 2025. doi: 10.1109/TETCI.2024.3502437.

LIU, M., Zeng, A., Chen, M., Xu, Z., LAI, Q., Ma, L., and Xu, Q. SCINet: Time series modeling and forecasting with sample convolution and interaction. In Oh, A. H., Agarwal, A., Belgrave, D., and Cho, K. (eds.), *Advances in Neural Information Processing Systems*, 2022.

Liu, Y., Hu, T., Zhang, H., Wu, H., Wang, S., Ma, L., and Long, M. itransformer: Inverted transformers are effective for time series forecasting. *arXiv preprint arXiv:2310.06625*, 2023.

Luo, D. and Wang, X. Deformablest: Transformer for time series forecasting without over-reliance on patching. In Globerson, A., Mackey, L., Belgrave, D., Fan, A., Paquet, U., Tomczak, J., and Zhang, C. (eds.), *Advances in Neural Information Processing Systems*, volume 37, pp. 88003–88044. Curran Associates, Inc., 2024.

Luo, Z., Huang, Y., Li, S., Wang, L., and Tan, T. Unfolding the alternating optimization for blind super resolution. *Advances in Neural Information Processing Systems (NeurIPS)*, 33, 2020.

Newey, W. K. and West, K. D. A simple, positive semi-definite, heteroskedasticity and autocorrelation consistent covariance matrix. *Econometrica*, 55(3):703–708, 1987. ISSN 00129682, 14680262.

Nie, Y., H. Nguyen, N., Sinthong, P., and Kalagnanam, J. A time series is worth 64 words: Long-term forecasting with transformers. In *International Conference on Learning Representations*, 2023.

Oreshkin, B. N., Carpov, D., Chapados, N., and Bengio, Y. N-beats: Neural basis expansion analysis for interpretable time series forecasting. In *International Conference on Learning Representations*, 2020.

Qiu, X., Wu, X., Lin, Y., Guo, C., Hu, J., and Yang, B. Duet: Dual clustering enhanced multivariate time series forecasting. In *SIGKDD*, pp. 1185–1196, 2025.

Razaviyayn, M., Hong, M., and Luo, Z.-Q. A unified convergence analysis of block successive minimization methods for nonsmooth optimization. *SIAM Journal on Optimization*, 23(2):1126–1153, 2013. doi: 10.1137/120891009.

Razaviyayn, M., Hong, M., Luo, Z.-Q., and Pang, J.-S. Parallel successive convex approximation for nonsmooth nonconvex optimization. In Ghahramani, Z., Welling, M., Cortes, C., Lawrence, N., and Weinberger, K. (eds.), *Advances in Neural Information Processing Systems*, volume 27. Curran Associates, Inc., 2014.

Reddi, S. J., Kale, S., and Kumar, S. On the convergence of adam and beyond. In *International Conference on Learning Representations*, 2018.

Shang, C., Chen, J., and Bi, J. Discrete graph structure learning for forecasting multiple time series. In *International Conference on Learning Representations*, 2021.

Sims, C. A. Macroeconomics and reality. *Econometrica*, 48(1):1–48, 1980. ISSN 00129682, 14680262.

Vaswani, A., Shazeer, N., Parmar, N., Uszkoreit, J., Jones, L., Gomez, A. N., Kaiser, L. u., and Polosukhin, I. Attention is all you need. In Guyon, I., Luxburg, U. V., Bengio, S., Wallach, H., Fergus, R., Vishwanathan, S., and Garnett, R. (eds.), *Advances in Neural Information Processing Systems*, volume 30. Curran Associates, Inc., 2017.

Wang, S., Wu, H., Shi, X., Hu, T., Luo, H., Ma, L., Zhang, J. Y., and ZHOU, J. Timemixer: Decomposable multi-scale mixing for time series forecasting. In *The Twelfth International Conference on Learning Representations*, 2024.

Wu, H., Xu, J., Wang, J., and Long, M. Autoformer: Decomposition transformers with auto-correlation for long-term series forecasting. In Beygelzimer, A., Dauphin, Y., Liang, P., and Vaughan, J. W. (eds.), *Advances in Neural Information Processing Systems*, 2021.

Wu, H., Hu, T., Liu, Y., Zhou, H., Wang, J., and Long, M. Timesnet: Temporal 2d-variation modeling for general time series analysis. In *International Conference on Learning Representations*, 2023.

Yu, B., Yin, H., and Zhu, Z. Spatio-temporal graph convolutional networks: A deep learning framework for traffic forecasting. In *Proceedings of the 27th International Joint Conference on Artificial Intelligence (IJCAI)*, 2018.

Yue, W., Liu, Y., Li, H., Wang, H., Ying, X., Guo, R., Xing, B., and Shi, J. Olinear: A linear model for time series forecasting in orthogonally transformed domain. *arXiv preprint arXiv:2505.08550*, 2025.

Zeng, A., Chen, M., Zhang, L., and Xu, Q. Are transformers effective for time series forecasting? *Proceedings of the AAAI Conference on Artificial Intelligence*, 37(9):11121–11128, Jun. 2023.

Zeng, J., Lau, T. T.-K., Lin, S., and Yao, Y. Global convergence of block coordinate descent in deep learning. In Chaudhuri, K. and Salakhutdinov, R. (eds.), *Proceedings of the 36th International Conference on Machine Learning*, volume 97 of *Proceedings of Machine Learning Research*, pp. 7313–7323. PMLR, 09–15 Jun 2019.

Zhang, Y. and Yan, J. Crossformer: Transformer utilizing cross-dimension dependency for multivariate time series forecasting. In *The Eleventh International Conference on Learning Representations*, 2023.

Zhou, H., Zhang, S., Peng, J., Zhang, S., Li, J., Xiong, H., and Zhang, W. Informer: Beyond efficient transformer for long sequence time-series forecasting. In *The Thirty-Fifth AAAI Conference on Artificial Intelligence, AAAI 2021, Virtual Conference*, volume 35, pp. 11106–11115. AAAI Press, 2021.

Zhou, T., Ma, Z., Wen, Q., Wang, X., Sun, L., and Jin, R. FEDformer: Frequency enhanced decomposed transformer for long-term series forecasting. In *Proc. 39th International Conference on Machine Learning (ICML 2022)*, 2022.

A. Dataset Details

Dataset	Variates	Freq.	Input Len.	Pred. Len.	Domain
ETTh1	7	Hourly	512	96–720	Electricity
ETTh2	7	Hourly	512	96–720	Electricity
ETTm1	7	15 min	512	96–720	Electricity
ETTm2	7	15 min	512	96–720	Electricity
Weather	21	10 min	512	96–720	Weather
Electricity	321	Hourly	512	96–720	Electricity
Traffic	862	Hourly	512	96–720	Transport

Table 3. Dataset statistics.

We evaluate long-term forecasting performance on seven widely used multivariate benchmarks: **Weather**, **Traffic**, **Electricity**, and the ETT family (**ETTh1**, **ETTh2**, **ETTm1**, **ETTm2**). These datasets are standard in the LTSF community and cover diverse domains including weather monitoring, traffic flow, and energy consumption. Following the established protocol of [Nie et al. \(2023\)](#); [Wu et al. \(2021\)](#), we split the data chronologically into training/validation/test sets with a ratio of 6:2:2 for the ETT datasets and 7:1:2 for the others. The input length is fixed to 512 across all experiments, and prediction horizons are {96, 192, 336, 720}. Key statistics are summarized in Table 3.

Weather. Records 21 meteorological indicators (e.g., temperature, humidity, wind speed) every 10 minutes throughout 2020 in Germany.

Traffic. Hourly road occupancy rates measured by 862 sensors on San Francisco Bay Area freeways between 2015 and 2016.

Electricity. Hourly electricity consumption (kWh) of 321 customers from 2012 to 2014.

ETT. The Electricity Transformer Temperature datasets include two hourly datasets (ETTh1, ETTh2) and two 15-minute datasets (ETTm1, ETTm2). Each contains seven oil temperature and load features collected from electricity transformers between July 2016 and July 2018.

B. Extended Gradient-Variance Plots

B.1. Prediction length = 96

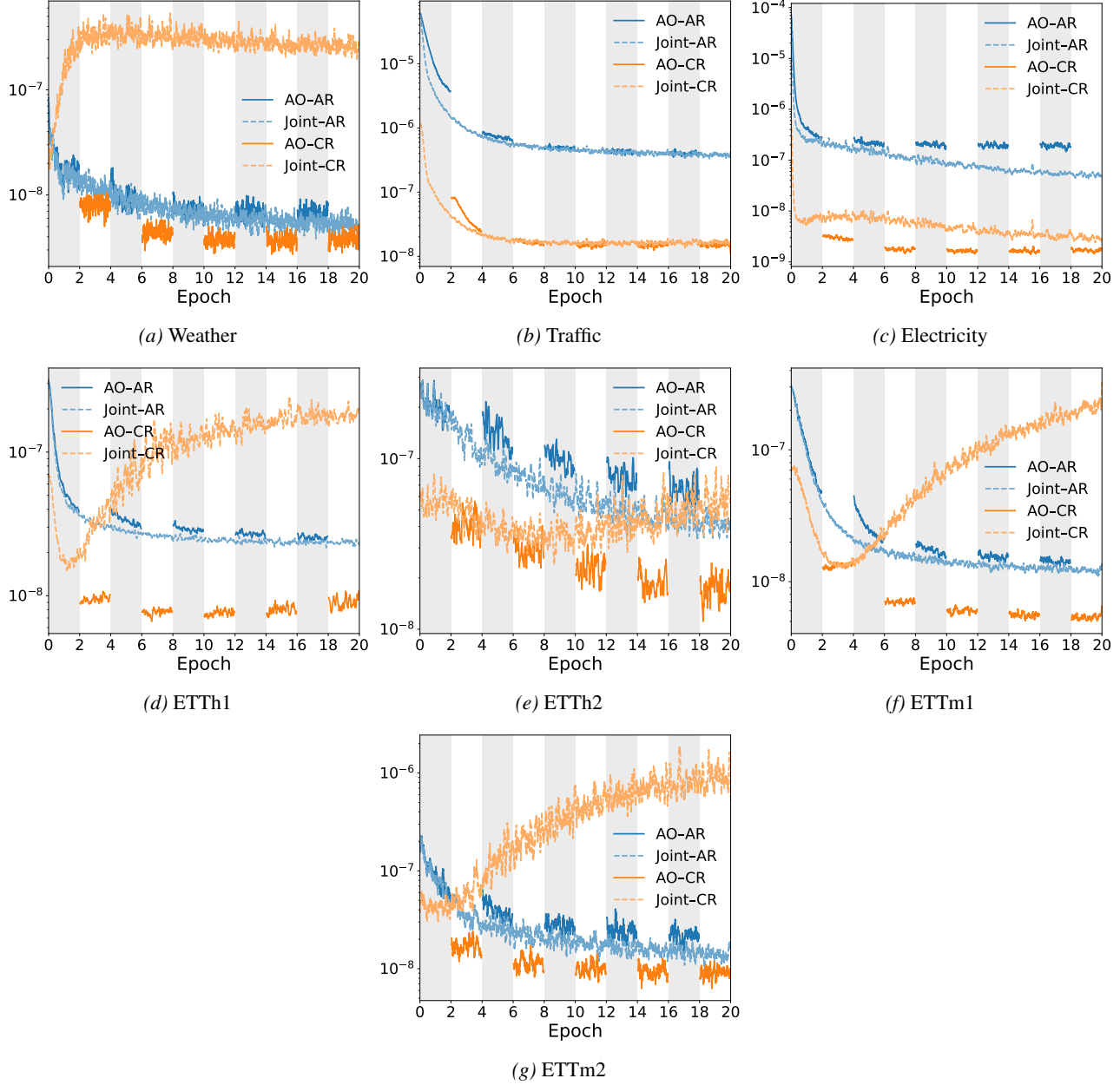


Figure 3. Prediction length = 96. Variance of AR/CR gradients under joint training across seven datasets. Higher variance indicates greater training instability, motivating alternating optimization in AltTS.

B.2. Prediction length = 192

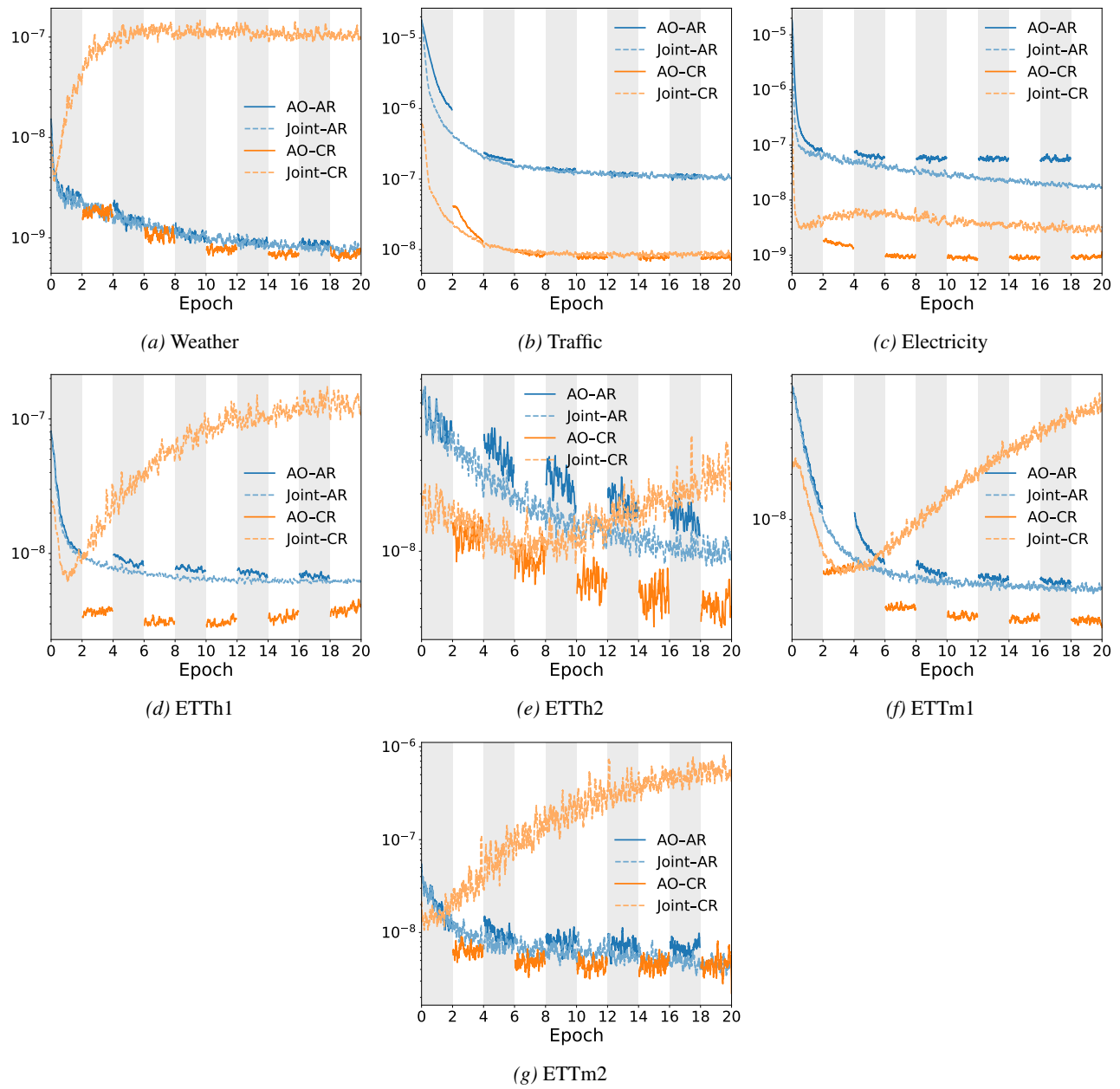


Figure 4. Prediction length = 192. Variance of AR/CR gradients under joint training across seven datasets.

B.3. Prediction length = 336

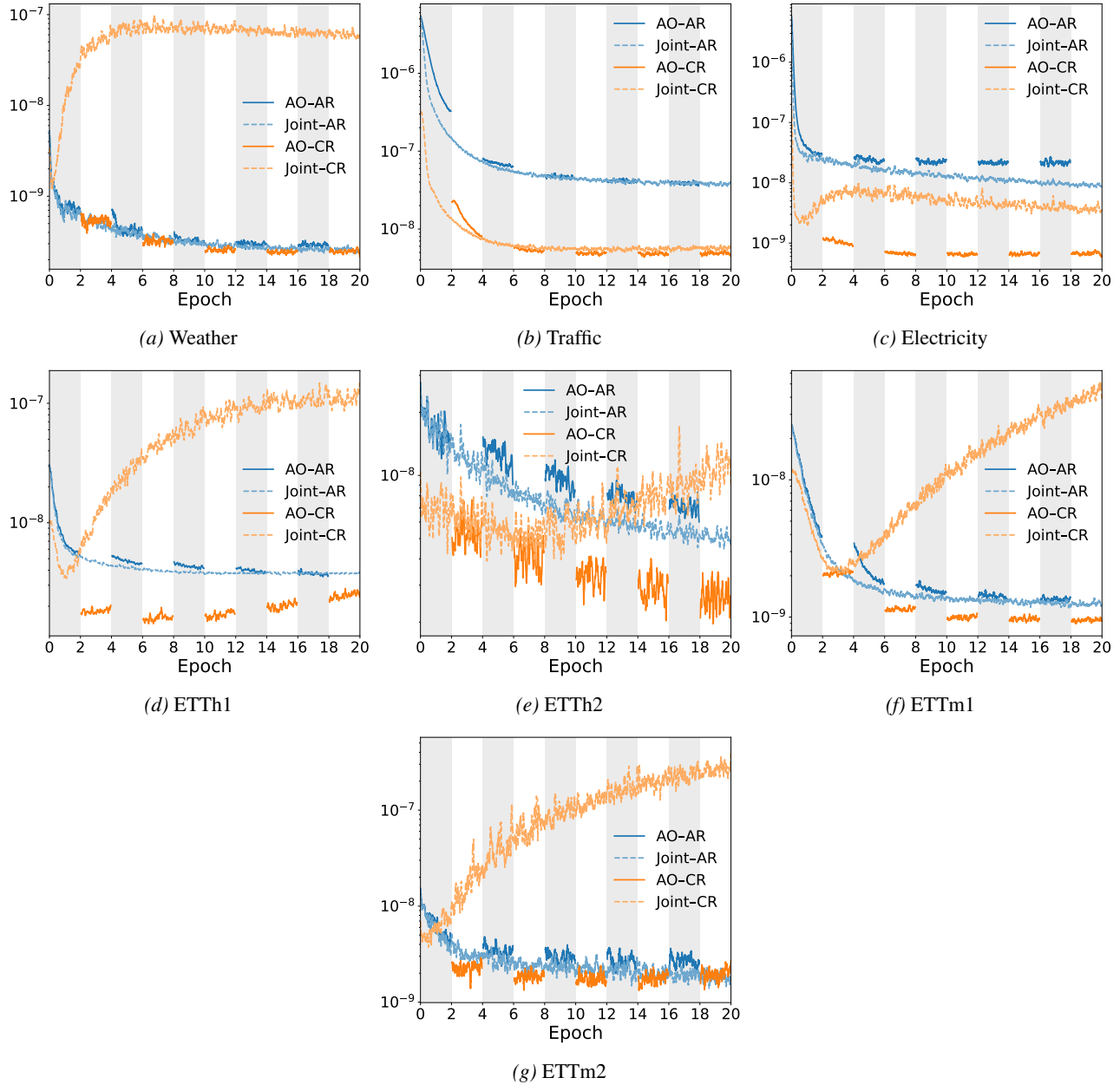


Figure 5. **Prediction length = 336.** Variance of AR/CR gradients under joint training across seven datasets.

B.4. Prediction length = 720

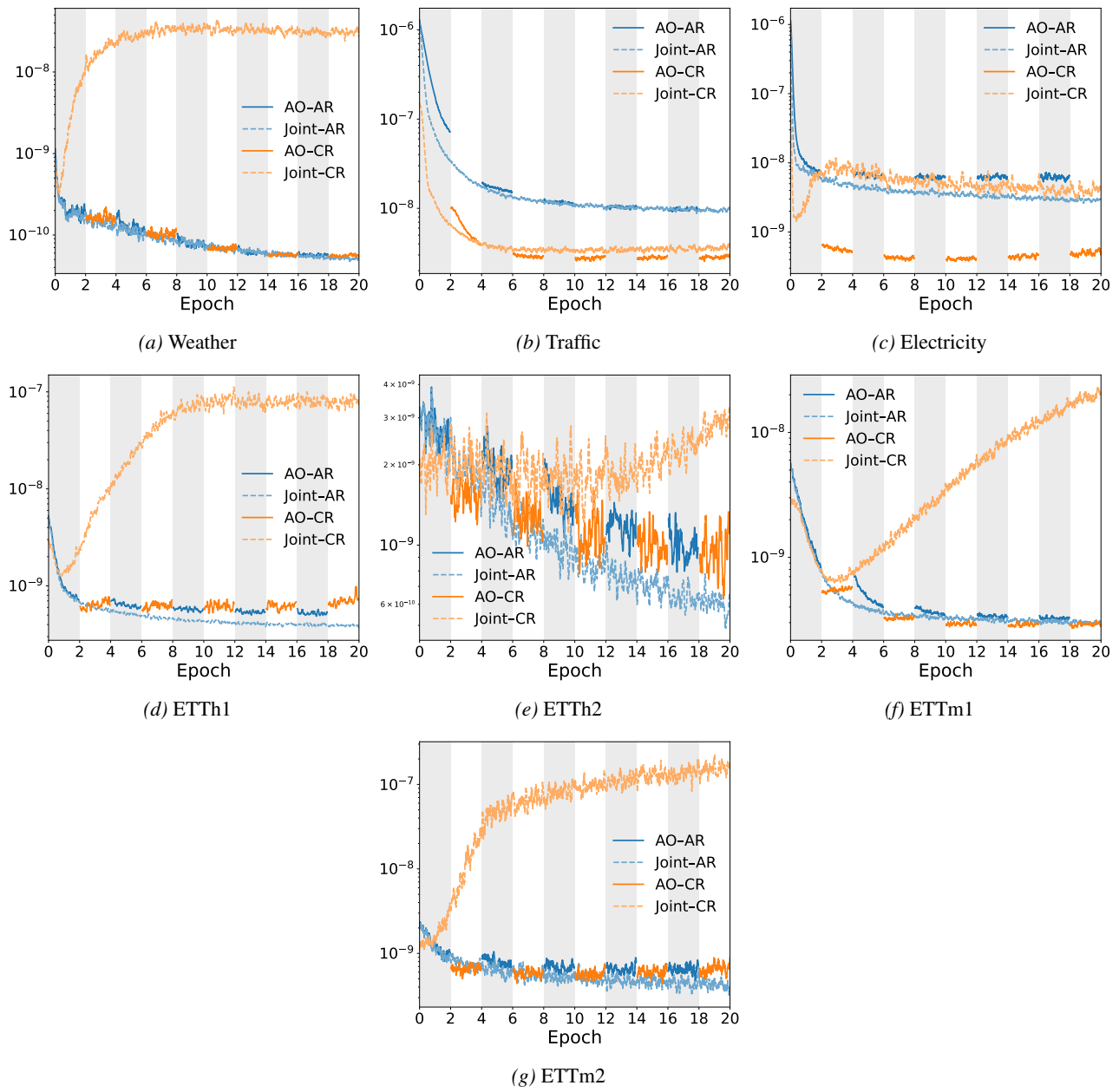


Figure 6. Prediction length = 720. Variance of AR/CR gradients under joint training across seven datasets.